**DTU Library**

**DTU**

# Geostatistical modelling of the spatial life history of post-larval deepwater hake Merluccius paradoxus in the Benguela Current Large Marine Ecosystem

Jansen, T; Kristensen, K; Fairweather, T. P.; Kainge, Paulus Inekela; Kathena, JN; Durholtz, M.D.; Beyer, Jan ; Thygesen, Uffe Høgsbro

[Link back to DTU Orbit](Link back to DTU Orbit)

1 **Geostatistical modelling of the spatial life history of post-larval deep-water hake**
2 (***Merluccius paradoxus***) **in the Benguela Current Large Marine Ecosystem**

3

4 Teunis Jansen[1,5] and Uffe Høgsbro Thygesen[5]

5 The following scientists contributed to the study but time constraints has not permitted them to
6 comment the final version of this working document: Kasper Kristensen[5], Paulus Kainge[2], Deon
7 Durholtz[3], Tore Strømme[4], John Kathena[2], Tracey P. Fairweather[3], Jan E. Beyer[5]

8

9     1)   BCC – Benguela Current Commission, Private Bag 5031, Swakopmund, Namibia.
10     2)   MFMR – Ministry of Fisheries and Marine Resources, PO Box 912, Swakopmund, Namibia.
11     3)   DAFF – Department for Agriculture, Forestry & Fisheries, Cape Town, South Africa.
12     4)   Institute of Marine Research, P.O. Box 1870 Nordnes, N-5817 Bergen, Norway.
13     5)   DTU AQUA – National Institute of Aquatic Resources, Charlottenlund, Denmark

14
15
16
17
18
19
20

24 Corresponding author: Teunis Jansen; DTU AQUA - *National Institute of Aquatic Resources,*
25 *Technical University of Denmark; Charlottenlund castle, 2920 Charlottenlund, Denmark; Tel.:*
26 *+4530667840; Fax: +4533963333; E-mail address:* Tej@aqua.dtu.dk*.*

27

28

## 1. Introduction

29

30  Deep-water hake (*Merluccius capensis*) is among the dominant demersal fish species in the

31  Benguela Current Large Marine Ecosystem (BCLME), a productive upwelling system off the

32  west coast of Southern Africa (5-37ºS, 0-26ºE). *M. paradoxus* inhabit the continental shelf slope

33  from around 17ºS in Angola/Namibia to about 27ºE in South Africa (Figure 1) (Payne, 1995).

34

35  *M. paradoxus* spawn mainly in areas of 200–650 m bottom depths between 34.5ºS and

36  36.5ºS on the South African west coast. Spawning individuals has been found as far as 25ºS in

37  Namibia and 27ºE off the South African south coast at depths ranging from 170 to 837 m (Jansen

38  et al., 2015a). Spawning off the South African coast takes place throughout the year, with

39  increased intensity around March and August–October (Jansen et al., 2015a).

40  Onshore, Offshore and alongshore ontogenetic migration has been indicated for *M.*

41  *paradoxus* (Le Clus et al., 2005; Strømme et al., 2016). Based on catch rates by length class from

42  South African surveys between 1990 and 2003, Le Clus et al (2005) concluded that *M.*

43  *paradoxus* on the west and south coast was connected and likely belonged to the same stock.

44  Strømme et al. (2016) extended this view to include Namibia where they found a large

45  proportion of late juveniles, indicating a southern origin and a subsequent spawning migration to

46  back to South Africa as the hakes matured. Juveniles initially migrate to shallower waters

47  followed by a lifelong movement towards deeper waters (Botha, 1980; Burmeister, 2001; Gordoa

48  and Duarte, 1991; Payne and Punt, 1995; Strømme et al., 2016). Large *M. paradoxus* has been

49  found down to 1000 m (Burmeister, 2001; Mas-Riera, 1991).

50  The spatio-temporal spawning and migration patterns are in accordance with the most recent

51  and comprehensive genetic study of *M. paradoxus* that found no spatial divergence and

52  concluded in accordance with (Bloomer et al., 2009) that the population structure is one

53  panmictic stock (Henriques et al., 2016). The authors found significant temporal divergence and

54  suggested that this was from genetic chaotic patchiness. An earlier study had pointed towards

55  multiple stocks (von der Heyden et al., 2010).

56  The area around the Lüderitz upwelling cell and Orange River Cone (LUCORC) region (25º-

57  29ºS) forms a natural barrier between the northern Benguela and southern Benguela (Agenbag

58  and Shannon, 1988; Lett et al., 2007; Rae, 2005). Therefore, and for practical/political simplicity,

59  the national border between Namibia and South Africa (Orange River at 29 ºS) is still regarded

60  as the boundary dividing the *M. paradoxus* into two management stocks (Figure 1) (Burmeister,

61  2005; Grant et al., 1988, 1987). The stock assessment and fisheries management advice has not

62  yet adopted to the new understanding of *M. paradoxus* as one panmictic stock that migrate across

63  the border between Namibia and South Africa. It is therefore unknown if the current fisheries

64  practice for *M. paradoxus* in the BCLME is sustainable and optimal.

65      Recent developments in geostatistics and model fitting has facilitated analyses of large

66  datasets from trawl surveys and let to new biological insight (Jansen et al., 2016, 2014;

67  Kristensen et al., 2014).

68      In the present study we apply these methods to a large dataset of survey data from Namibia

69  and South Africa to exhibit the spatial life history of post-larval *M. paradoxus*. This is the first

70  analysis of *M. paradoxus* integrated both the South African, Namibian and Norwegian surveys.

71      We aim to test if the data supports the hypothesis of one panmictic stock and transboundary

72  migration. Furthermore, we quantify the size specific migration for future usage in improved

73  stock assessments.

74

75  **2 Materials and methods**

76

77  The data used for this study were the same as used by Jansen et al. (2016), except that data from

78  2012 were not available for *M. paradoxus*. Modelling, post-processing and presentation of the

79  results also followed the methods and design described in Jansen et al. (2016). The following

80  description of materials and methods is therefore a modified copy from Jansen et al. (2016).

81  *2.1 Scientific trawl survey data*

82      The dataset used in this study comprised data from demersal trawl surveys conducted during

83  the period 1998–2011 in the Benguela-Agulhas ecosystem between 17°S (northern border of

84  Namibia) and 27°E on the South African south coast (Figure 1). All surveys sampled the

85  demersal fish community on the continental shelf and upper shelf slope.

86  Namibian surveys used a Gisund Super demersal trawl towed by chartered commercial

87 trawlers, all inter-calibrated with the *R/V Dr Fridtjof Nansen*, and the data were made available

88 by the Ministry of Fisheries and Marine Resources (MFMR) in Namibia. Namibia surveys

89 followed a systematic transect design with resampling of fixed transects with a semi-random

90 distribution of stations along the transects. The South African surveys were conducted using

91 either the "old" or the "new" configuration of a German 4-panel bottom trawl onboard *R/V*

92 *Africana*. A few surveys were also conducted in South African waters using the Gisund trawl

93 onboard *R/V Dr. Fridtjof Nansen*. South Africa surveys followed a random stratified sampling

94 survey design. Details on the three types of gear, their operation and rigging are available in

95 Axelsen and Johnsen (2015). Trawling time was approximately 30 minutes, and data from hauls

96 shorter than 25 mins or longer than 35 were excluded from the analysis. Data from *R/V Africana*

97 were made available by the Department of Agriculture Forestry and Fisheries (DAFF) in South

98 Africa and data from *R/V Dr. Fr. Nansen* were provided by FAO/Norway (IMR). No trawl

99 samples were available from Angolan waters due to species identification problems between *M.*

100 *capensis*, *M. paradoxus* and *M. polli* (Benguela hake, which is largely caught in Angola).

101  For each trawl haul, the total catch was weighed and sorted to species level where possible.

102 Large catches were subsampled. The weight of all *M. capensis* in the catch was recorded and

103 total lengths of a subset of the individuals were measured in cm (rounded down). The length data

104 recorded from the subsamples were subsequently raised to estimate the length composition in the

105 total catch.

106  Data collected from nine hauls where winds in excess of 25 knots may have compromised

107 the performance of the gear and hence the associated data points (Wieland et al., 2013) were

108 excluded from the dataset.

109  The final survey dataset comprised 6 343 trawl hauls from 1998 to 2011, 57 % of which

110 contained *M. paradoxus*. Catches (in numbers) ranged from 0 to 29 844 *M. paradoxus* per haul,

111 with a mean catch of 867 in the non-zero hauls. The data set comprised a total of 3.1 million

112 records of *M. paradoxus* lengths. Samples were available from the entire region except the

113 shallow area (20 - 100 m) in central Namibia that is characterized by untrawlable bottom (Figure

114 1). The samples were relatively equally distributed over the time-series (Fig. 2a). Most samples

115 in Namibia and on the South African west coast were taken in January-February, while the South

116 African south coast was generally sampled in April-May (Figure 2b). Trawling was
117 predominately done during the day (Figure 2c) at depths from 20 to 960 m (Figure 2d). The catch
118 numbers from gears other than Gisund (i.e. "old" Africana and "new" Africana) were
119 deterministically converted to the Gisund equivalent catch using the estimated length-specific
120 gear effect from supplementary information 1.

121    The difference in the timing of the surveys in the various sub-regions in addition to the
122 spawning phenology made it impossible to estimate the exact age of the hakes. M. paradoxus
123 spawn throughout the year with increased intensity around March and August–October (Jansen
124 et al., 2015a). The northern parts of the region (central Namibia) were surveyed in January to
125 February (mean = 30 January). Consequently, the recruits in Namibia were primarily surveyed
126 approximately 4.5 and 10.5 months after spawning. The South African west coast was also
127 surveyed in January to February. Off the South African south coast surveys took place three
128 months later (April-May, mean = 26 April). The young-of-the-year hake therefore entered the
129 survey catches at various sizes and ages. For illustration purposes, mean age of the young-of-the-
130 year hakes that entered the catches were set to 6 months.

131 *2.2 The GeoPop model*

132    Log Gaussian Cox (LGC) process modelling with correlations was used to describe
133 abundance indices of *M. paradoxus* cohorts through space and time and along environmental
134 gradients, observed using various gear types, as the hake recruited, grew and died. Similar
135 models have previously proved their value for mackerel larvae and juveniles (Jansen et al.,
136 2015b, 2012), cod (*Gadus morhua*) (Kristensen et al., 2013; Lewy and Kristensen, 2009),
137 whiting (*Merlangius merlangus*) (Nielsen et al., 2014), and shallow-water hake (*Merluccius
138 capensis*) (Jansen et al., 2016).

139    The first attempts to fit this type of model to the hake data from demersal surveys were
140 unsuccessful because the large number of latent variables that needed to be estimated in this 4D-
141 problem exceeded the limits of the physical processing power. The recent advent of the Template
142 Model Builder (TMB; Kristensen et al., 2015) – a software library that can fit random effect
143 models much faster than AD model Builder (Fournier et al., 2012)  provided a solution to this
144 obstacle. Physical processing power was furthermore increased by running the software on an
145 r3.8xlarge instance under Amazon Elastic Compute Cloud (Amazon EC2). TMB was installed

146   on Linux on the r3.8xlarge platform consisting of 32 CPUs (2.5 GHz Intel Xeon E5-2670 v2,

147   AVX and turbo boost), 244 GiB RAM and 2 x 320 GB SSD storage

148   (https://aws.amazon.com/ec2/instance-types/). This setup facilitated the study of *M. capensis* in a

149   rich dataset by a complex model – a study that was impossible with ADMB or the model fitting

150   algorithms provided in the LGC-package used by Kristensen et al. (2013). The same setup was

151   used in the present study of *M. paradoxus.*

152        The model formulation and notation used for this study was identical to that described by

153   Kristensen et al. (2013). The response variable was catch in numbers from 47 size classes (2 cm

154   bins from 5 to 99 cm) in annual time steps in the period 1998 to 2011. The model consisted of

155   four main elements: The large scale spatio-temporal aspects ($\eta(s,x,t)$), the local patchiness

156   ($\eta_0(s,j)$, the population dynamics size-spectrum ($\phi(s,t)$) and the gear selectivity ($sel(s)$).

157   In the log-domain, the sum of these four components equals the total (latent) log intensity of the

158   poisson measurements indexed by haul-id *j*:

159        $\log(\lambda(s_j,x_j,t_j)) = \eta(s_j,x_j,t_j) + \eta_0(s_j,j) + \phi(s_j,t_j) + \log(sel(s_j))$ For the first three

160   elements the variance parameters are denoted by $\sigma^2$, $\sigma_N^2$ and $\sigma_\varepsilon^2$, respectively. Conditional on

161   the intensity *λ*, the counts (i.e. the number of *M. paradoxus* in each size class in a haul taken at a

162   particular point in space and time, with a particular gear) were assumed to be Poisson distributed

163   (Kristensen et al., 2013). This implied a resulting (unconditional) distribution with much higher

164   dispersion than the Poisson. This model structure is referred to as a log Gaussian Cox process

165   model and has been shown to be appropriate for count data from catches that are over-dispersed

166   and zero-inflated (with many zero values) (Jansen et al., 2015b; Kristensen et al., 2013). The

167   Poisson distribution allows for zero catches, while the log Gaussian randomness imply over-

168   dispersed catches (relative to Poisson), both allowing for very high counts and for many more

169   zero catches than would be found in a pure Poisson model.

170        The large scale spatio-temporal element ($\eta(s,x,t)$) was a key feature of the model. It

171   models the time-varying heterogeneous spatial distribution of a size-structured population. The

172   statistical properties of this distribution were modelled in three parts: large-scale spatial patterns

173   (correlations between cells), temporal fluctuations (correlations between years) and size structure

174   (correlations between catches in different size classes). All correlations were assumed to decay

175   exponentially with spatial distance, time lag, and size difference, respectively, and assumed to be

176    multiplicative. The spatial correlation was assumed to be isotropic (direction independent). In

177    order to avoid correlation over land (e.g. the Cape region in South Africa), the spatial correlation

178    effect was modelled as a Gaussian Markov random field (cell-to-cell chains). The parameter

179    estimates for these correlations were expressed as decorrelation distance ($H$), decorrelation time

180    ($T$) and decorrelation size ($L$), which were the distances in space, time or size where the

181    correlations had decayed to $e^{-1}$ (explaining ca. 14% of the variance). Documentation of these

182    correlation structures were published in Kristensen *et al.* (2013). The spatio-temporal fields were

183    represented by annual time steps covering the 14 years of the study period (1998 – 2011) and the

184    spatial grid consisted of 278 cells each measuring $50 \times 50$ km. The large scale spatio-temporal

185    model element therefore consisted of 182 924 random variables (47 size class × 14 years × 278

186    grid cells), which were assumed to follow a log Gaussian distribution that determined the mean

187    of the catch (in numbers).

188        The second main element in the model, which reflected local patchiness and fish' tendency to

189    aggregate with similar sized individuals on a local scale was the "nugget effect" ($\eta_0(s, j)$). It is

190    a well-known phenomenon that catches of certain fish sizes tend to be overrepresented in trawl

191    hauls compared to the size distribution in the sampled population in the sea, likely due to the

192    size-structured nature of schools or shoals (Kristensen et al., 2013). This local effect was

193    accounted for by modelling the remaining variation among the hauls (within cells) with a

194    Gaussian-distributed mean-zero term of variance $\sigma_N^2$ and decorrelation range ($L$) across sizes.

195        The third main element of the model was the stochastic population dynamics size spectrum

196    ($\phi(s, t)$). It was governed by the McKendrick-von Foerster equation ($\frac{\partial \phi}{\partial t} = -g \frac{\partial \phi}{\partial s} - z$) (Kot,

197    2001) with an added noise term ($\varepsilon$) applied in every time step to make this model much more

198    flexible than the deterministic counterpart (Kristensen et al., 2013).  The constant growth and

199    mortality rates should therefore be interpreted as averages rates over time. The population

200    dynamics were discretized into 47 size classes and 32 time steps per year. Consequently, this was

201    represented by 21 056 random effects (47 size class × 14 years × 32 time steps).

202

203        Finally the catch was affected by the catchability of the gear (*sel(s)*) and this effect was

204    implemented as:

205 $$sel(s) = (1 + 3^{-(2/SR)*(s-\ell_{50}^{Gisund})})^{-1},$$

206 where *sel(s)* was the selection factor, *SR* was the selection range and $\ell_{50}^{Gisund}$ was the fish length

207 (*s*) in cm at half selection for the Gisund gear.

208 The parameters in the model were estimated using the maximum likelihood principle based

209 on the Laplace approximation and thus the estimation follows the principles of Kristensen et al.

210 (2013).

211 The fitted model was then used to calculate annual estimates of the abundance index of hake

212 in each size class in each 50 x 50 km cell. These spatio-temporal distribution patterns were also

213 transformed into a coastline-oriented coordinate system, to reveal any along-shore migration

214 patterns. This was done by projecting the estimated abundances in the Cartesian coordinate

215 system onto an axis that followed the coastline as a straight line from the Namibia-Angola border

216 (11°E , 17°S) in the North, via Cape Point (18.5°E, 34°S) to east of Port Elizabeth on the South-

217 African south coast (27.5°E, 34°S) (see Fig. 1). Multiannual average distributions were

218 calculated as the unweighted average distribution of multiple years.

219 For explanatory purposes, the length-based model outputs were presented by both length and

220 absolute age. The length-to-age conversions were done by using the age readings by DAFF (D.

221 Durholtz, DAFF, unpublished data). This was done by calculating the average age by length

222 from the Von Bertalanffy equations fitted to age readings of male and female *M. capensis*,

223 respectively (plot provided in results section). Maps and bar plots were constructed to show

224 mean distributions of *M. capensis* of length groups corresponding (+/- 1.5 cm) to the ages in one

225 year steps from 0.5, the mean size and age when a new cohort first appears in the surveys, to 9.5

226 years.

227 Depth data were downloaded as gridded (0.07° lat x 0.07° lon) averages from the NOAA

228 ETOPO1 database (Amante and Eakins, 2009) using the "marmap" package (Pante et al., 2015).

229 Mean depth was calculated for each cell and isobaths were produced for the maps. Finally,

230 abundance in cells with a mean depth exceeding the deepest trawl haul (960 m) was set to 0. The

231 deepest observed *M. paradoxus* catch was at 934 m.

232

233     **3. Results**

234         The parameter estimates (and associated standard errors) of the model fitted to the catch data

235     are given in Table 1.

236         Hake densities were found to be correlated in space and size with a spatial de-correlation

237     distance (*H*) of 481 km and a length de-correlation difference (*L*) of 79 cm. These patterns were

238     found to be very stable from year to year with a temporal de-correlation period (*T*) spanning 30.1

239     years (CV = 7 %) and could therefore be examined as averages over the entire time series.

240         Estimated variance parameters revealed a roughly equal contribution from spatial large-scale

241     patterns ($\sigma^2$ = 20.9) and the nugget effect ($\sigma_N^2$ = 12.4). In comparison, the contribution from

242     population dynamics was much smaller ($\sigma_\varepsilon^2$ = 0.03). The variance in abundance of a given size

243     class at a single point in time and space was therefore completely dominated by large scale

244     spatial effects and local effects rather than demographic effects.

245         The total mortality rate of *M. paradoxus* was estimated to 0.33 year$^{-1}$ (CV = 67 %).

246     However, this varied through life and between areas. The mortality increased substantially when

247     the fish exceeded approximately 55 cm (Figure 3). The growth rate was estimated to be 8.3 cm

248     year$^{-1}$ (CV = <0.001 %). Despite the very weak population effect, these estimates (mortality and

249     growth) resembled previously reported rates (Figure 3 and 4). However, the cohort signals were

250     too weak to be used for tracking of single cohorts and their effects on spatio-temporal

251     distribution fields were negligible.

252         *M. capensis* was not fully recruited to the trawl survey in their first year (Figure 3). This was

253     evident from the estimated selection of the reference gear "Gisund" ($\ell_{50}^{Gisund}$ = 8.4 cm, $SR^{Gisund}$

254     = 1.4 cm) and the increase in abundance from 0.3 to 1.3 years (Figure 3).


255     *3.1 Spatial patterns (distribution, migration, population structure)*

256         The spatial distribution of the catch rate of *M. paradoxus* was estimated and illustrated to

257     infer age and size-related migration patterns. This was done for length groups corresponding to

258     the ages from 0.3, the approximate age when a new cohort first appears in the surveys, to 9.3

259     years.

260         To examine the alongshore migration patterns, we projected the length-age-specific spatial

261     distributions onto an axis consisting of two straight lines, one from the Namibia-Angola border

262 (Kunene River mouth) in the North, via Cape Point to Port Elizabeth in the south-east. The

263 alongshore projections (Figure 5 and 6) and distribution maps (Figure 7 and 8) indicated

264 horizontal movements throughout the life span of *M. paradoxus*. The initial distributions of the

265 approximately 0.3- year-olds (recruits) and the 1.3-years olds (juveniles) indicated one main

266 nursery area (Figure 6 and 7). During the first 7 years of the life of *M. paradoxus*, the

267 distribution shifted gradually from year to year, indicating considerable alongshore migrations.

268 In the north, considerable quantities of *M. paradoxus* appeared to move northwards from the area

269 around Orange River - their most likely origin. In lesser number, *M. paradoxus* moved eastwards

270 along the south coast of South Africa. *M. paradoxus* were most widespread at the age of

271 approximately 4.3 years (51 cm) where almost 100 % were mature (50 % mature at 42 cm (Singh

272 et al., 2011)). Later, the distributions progressively contracted in the vicinity of the nursery area

273 (Figure 5, 6 and 8). The movements north of Orange River (the border between Namibia and

274 South Africa) and east of Agulhas thus indicated natal homing as the most parsimonious

275 explanation. Consequently, transboundary movements most likely occurred.

276 *M. paradoxus* appeared initially to move to shallower waters at around 80 m depth, after

277 which they gradually moved deeper from approximately 0.5 to 5 years of age. From the age of 5

278 they were found from 150 to 935 m, but mainly between 350 and 650 m, while moving into

279 slightly shallower waters (Figure 9).

280 **4. Discussion**

281 The present analysis was based on the hitherto largest database of *M. paradoxus* survey data,

282 for the first time including surveys from both the Namibian, Norwegian and South African

283 fisheries research institutes. The quantitative geostatistical modelling exposed spatial migration

284 patterns largely in line with Strømme et al. (2016) that were based on visual inspection of

285 presence/absence outline maps based. Like Strømme et al. (2016) and Le Clus et al. (2005) we

286 assumed that the spatial shifts in distribution over the life span of post-larval *M. paradoxus* were

287 primarily reflecting migration and to a lesser extent mortality, however, the effects of spatial

288 variation in mortality remains to be studied.

289    *4.1 Spatial patterns (distribution, migration, population structure)*

290    The results indicated one primary recruitment/nursery area on the west coast of South Africa

291    and a secondary low-production area around Port Elizabeth on the South Coast. Juveniles

292    initially migrated away from the main recruitment area, followed by natal homing by larger

293    individuals. This pattern was highly consistent through the studies time series as indicated by the

294    very long decorrelation time.

295    The return migration from Namibia appeared to take place when the hakes exceeded 50 cm.

296    At this size almost 100 % would be mature if they matured at the same size as in South Africa

297    Singh et al (2011), which is in contrast to the very few findings of spawning *M. paradoxus* in

298    Namibian waters (Jansen et al., 2015a). Size of maturation therefore needs to be estimated for the

299    part of the stock that migrates into Namibian waters.

300    At the South coast of South Africa *M. paradoxus* appeared to move slightly westwards and

301    then stay after reaching the size of maturation. This corresponds to the spawning reported in this

302    area by Jansen et al. (2015a). However, very few recruits were observed, indicating that either

303    they were outside the surveys area, transported by the currents to the west coast before they were

304    caught in the survey, underestimated (unaccounted gear avoidance due to factors such as vertical

305    distribution or gear), or the reproduction in this area was less successful than on the west coast.

306    The spatial life history patterns thus conform to the concept of one main population unit

307    (stock), but points to an additional smaller component on the eastern part of South Africa's south

308    coast. The level of interconnection (mixing/straying) between these components (stocks) is

309    presently unknown, but appears to exceed the threshold where genetic differentiation occurs in

310    the mitochondrial DNA (Henriques et al., 2016). Furthermore, the rarity of small juveniles in the

311    eastern survey catches is puzzling and calls for field work using other techniques than the

312    standard survey.

313    *M. paradoxus* reached its deepest distribution at around 50-55 cm length (Figure 9), where it

314    was abundant at depths deeper that 600 m. These depths were not completely covered by the

315    surveys. This corresponds to an increased mortality at the same sizes (Figure 3), which could be

316    explained by fish moving out of the survey coverage.

317

318    *4.2 Population dynamics and nugget effects*

319    The effect of the population dynamics in the model was minuscule, this could be a
320    consequence of the year-round spawning and recruitment of *M. paradoxus* combined with the
321    difference in timing of the South African South coast and West coast surveys. Despite this,
322    growth and mortality rates appeared to be relatively well estimated as indicated by the low
323    standard deviations of the estimates and the comparison with values reported from age readings
324    and stock assessments. A plausible explanation for this result, which is consistent with what was
325    found for *M. capensis* (Jansen et al., 2016),  is that the variability in the size-structured spatial
326    patterns is so relatively large, that the contribution from the population dynamics is not required
327    to explain patterns in data.

328

329    The data and model fit for *M. paradoxus* did not indicate any large spatial differences in
330    small scale variability (nugget effect) that complicated the interpretation of the model fit like for
331    *M. capensis* (Jansen et al., 2016). This is evident from supplementary information 2 that is made
332    for comparison with figure 5 and 6 in Jansen et al. (2016).

333

334    To be added: 1. Discuss gear effects. 2. Test sensitivity to the gear effect estimates. How much
335    would the results change if the gear effects changed (Supplementary information 3).

336

337    *4.2 Model performance and future developments*
338    The GeoPop model has been made possible by Template Model Builder's computational
339    approach to general statistical problems with many unobserved random variables, as well as the
340    availability of memory and processing power through cloud computing. GeoPop represents a
341    major improvement of earlier approaches, specifically by including both population dynamics,
342    large-scale spatial patterns, and small-scale size-structured clustering. Since GeoPop lies at the
343    boundary of what is currently computationally feasible, a number of compromises had to be
344    made with respect to the ecological fidelity of the model, and it is foreseeable that future
345    developments in algorithms and computational resources will allow further refinement of the
346    model assumptions. Here, we list three candidates for such refinements:

347     1.  Currently, the correlation structure in the spatial fields is assumed to be isotropic, i.e.
348         independent of direction. It is plausible that correlations between different locations
349         depend not only on distance, but also on differences in depth or other key habitat
350         parameters. Some extensions are relatively straightforward and could for example be
351         achieved by changing coordinates from latitude and longitude to alongshore distance and
352         depth. However, this solution would have other flaws, as it would e.g. regard an off-shore
353         bank as an extension of the near-coast space. A more general and robust structure could
354         be obtained by modelling the fluxes in space that drive the redistribution of the stock
355         between time points; this could include diffusive fluxes which would be anisotropic, as
356         well as advective fluxes which indicate preferred migrations. While such an extension is
357         appealing from the point of view of first principles in spatial ecology, by explicitly
358         modelling migrations, it would lead to correlation structures that make computations
359         much more demanding. In general, inference in spatiotemporal dynamics, including
360         model selection, is a computationally intensive task in which the trade-off between
361         fidelity and feasibility must constantly be reassessed as computational abilities expand.

362     2.  The growth dynamics and the mortality patterns are grossly simplified, in that both are
363         assumed constant. A major effort would be required to allow changes in growth rates,
364         explained by current size and possibly also environmental covariates, as well as varying
365         mortality, most importantly described by spatiotemporal patterns in fishing effort.
366         Ultimately, the inclusion of such patterns could lead to a spatiotemporal size-based
367         assessment model. The effort required for this development would be very substantial,
368         but single steps in this direction could be pursued.

369     3.  It could be envisioned to include different stock components, differing in timing and
370         location of spawning. This would facilitate the tracking of individual cohorts.

371

## 5. Conclusion

373     The perception of the migration and population patterns derived from the first geostatistical
374     modelling of data from all surveys in the region corresponds largely to the hypothesis and data

375    plots presented by Le Clus et al. (2005) and Strømme et al. (2016), but differ from the current

376    assessment practices in Namibia and South Africa, where two stocks are assumed to be separated

377    by the national border.

378

385

386

387

**References**

389 Agenbag, J.J., Shannon, L.V., 1988. A suggested physical explanation for the existence of a
390     biological boundary at 24 30′ S in the Benguela system. South African J. Mar. Sci. 6, 119–
391     132.

392 Amante, C., Eakins, B.W., 2009. ETOPO1 1 Arc-Minute Global Relief Model: Procedures, Data
393     Sources and Analysis. NOAA Tech. Memo. NESDIS NGDC-24 1–19.

394 Axelsen, B.E., Johnsen, E., 2015. An evaluation of the bottom trawl surveys in the Benguela
395     Current Large Marine Ecosystem. Fish. Oceanogr. 24, 74–87.

396 Bloomer, P., Santos, S., Oosthuizen, C., Hoareau, T., Klopper, A., 2009.  Hake population
397     genetics: development of microsatellite markers and screening of microsatellite locus
398     variation in Cape hakes, Merluccius paradoxus and M. capensis, from the Namibian and
399     South African coasts. BENEFIT Report, Univ. Pretoria, South Africa.

400 Botha, L., 1980. The biology of the Cape hake Merluccius capensis Cast. and M. paradoxus
401     Franca. PhD thesis, Stellenbosch Univ. South Africa.

402 Burmeister, L., 2005. Is there a single stock of Merluccius paradoxus in the Benguela
403     ecosystem? African J. Mar. Sci. 27, 23–32. doi:10.2989/18142320509504065

404 Burmeister, L., 2001. Depth-stratified density estimates and distribution of the Cape hake
405     Merluccius capensis and M. paradoxus off Namibia, deduced from survey data, 1990–1999.
406     S. Afr. J. Mar. Sci. 23, 347–356.

407 Fournier, D.A., Skaug, H.J., Ancheta, J., Ianelli, J., Magnusson, A., Maunder, M.N., Nielsen, A.,
408     Sibert, J., 2012. AD Model Builder: using automatic differentiation for statistical inference
409     of highly parameterized complex nonlinear models. Optim. Methods Softw. 27, 233–249.

410 Gordoa, A., Duarte, C.M., 1991. Size-dependent spatial distribution of hake (Merluccius
411     capensis and Merluccius paradoxus) in Namibian waters. Can J Fish Aquat Sci 48, 2095–
412     2099.

413 Grant, W.S., Becker, I.I., Lesliet, R.W., 1988. Evolutionary divergence between sympatric
414     species of southern African hake, Merluccius capensis. Heredity (Edinb). 61, 13–20.

415  Grant, W.S., Leslie, R.W., Becker, I.I., 1987. Genetic stock structure of the southern African

416      hakes Merluccius capensis and M. paradoxus. Mar. Ecol. Prog. Ser. 41, 9–20.

417  Henriques, R., von der Heyden, S., Lipinski, M.R., du Toit, N., Kainge, P., Bloomer, P.,

418      Matthee, C.A., 2016. Spatio-temporal genetic structure and the effects of long-term fishing

419      in two partially sympatric offshore demersal fishes. Mol. Ecol. doi:10.1111/mec.13890

420  Jansen, T., Kainge, P., Singh, L., Strömme, T., Durholtz, M.D., Kathena, J., Wilhelm, M.R.,

421      Erasmus, V., Beyer, J.E., 2015a. Spawning Patterns of Shallow-Water Hake (Merluccius

422      capensis) and Deep-Water hake (M. paradoxus) in the Benguela Current Large Marine

423      Ecosystem Shown by Gonadosomatic Index (GSI). Fish. Res. 172, 168–180.

424      doi:10.1016/j.fishres.2015.07.009

425  Jansen, T., Kristensen, K., Kainge, P., Durholtz, D., Strømme, T., Thygesen, U.H., Wilhelm,

426      M.R., Kathena, J., Fairweather, T.P., Paulus, S., Degel, H., Lipinski, M.R., Beyer, J.E.,

427      2016. Migration, distribution and population (stock) structure of shallow-water hake

428      (Merluccius capensis) in the Benguela Current Large Marine Ecosystem inferred using a

429      geostatistical population model. Fish. Res. 179, 156–167. doi:10.1016/j.fishres.2016.02.026

430  Jansen, T., Kristensen, K., Payne, M., Edwards, M., Schrum, C., Pitois, S., 2012. Long-term

431      Retrospective Analysis of Mackerel Spawning in the North Sea: A New Time Series and

432      Modeling Approach to CPR Data. PLoS One 7(6), 1–10. doi:10.1371/journal.pone.0038758

433  Jansen, T., Kristensen, K., van der Kooij, J., Post, S., Campbell, A., Utne, K.R., Carrera, P.,

434      Jacobsen, J.A., Gudmundsdottir, A., Roel, B.A., Hatfield, E.M.C., 2015b. Nursery areas and

435      recruitment variation of North East Atlantic mackerel (Scomber scombrus). ICES J.Mar.Sci.

436      72(6), 1779–1789. doi:10.1093/icesjms/fsu186

437  Jansen, T., Kristensen, K., van der Kooij, J., Post, S., Campbell, A., Utne, K.R., Carrera, P.,

438      Jacobsen, J.A., Gudmundsdottir, A., Roel, B.A., Hatfield, E.M.C., 2014. Nursery areas and

439      recruitment variation of Northeast Atlantic mackerel (Scomber scombrus). ICES J. Mar.

440      Sci. doi: 10.10, 11 pp. doi:10.1093/icesjms/fsu186

441  Kot, M., 2001. Elements of Mathematical EcologyCambridge University Press. New York.

442  Kristensen, K., Nielsen, A., Berg, C.W., Skaug, H., Bell, B., 2015. TMB: Automatic

443      Differentiation and Laplace Approximation. J. Stat. Softw. http://arx, 1–21.

444  Kristensen, K., Thygesen, U.H., Andersen, K.H., Beyer, J.E., 2014. Estimating spatio-temporal

445      dynamics of size-structured populations 336, 326–336.

446  Kristensen, K., Thygesen, U.H., Andersen, K.H., Beyer, J.E., 2013. Estimating spatial-temporal

447      dynamics of size-structured populations. Can J Fish Aquat Sci 99, 1–44.

448  Le Clus, F., Hennig, H..-K.O., Osborne, R.F., Leslie, R.W., 2005. Size-dependent spatial

449      dynamics of deep-water Cape hake Merluccius paradoxus density distribution on two

450      coasts, 1990-2003. Mar. Coast. Manag. South Africa, Demersal Work. Gr. Doc.

451      WG/02/05/D.

452  Lett, C., Veitch, J., van der Lingen, C.D., Hutchings, L., 2007. Assessment of an environmental

453      barrier to transport of ichthyoplankton from the southern to the northern Benguela

454      ecosystems. Mar. Ecol. Prog. Ser. 347, 247–259. doi:10.3354/meps06982

455  Lewy, P., Kristensen, K., 2009. Modelling the distribution of fish accounting for spatial

456      correlation and overdispersion. Can. J. Fish. Aquat. Sci. 66, 1809–1820.

457  Mas-Riera, J., 1991. Changes during growth in the retinal structure of three hake species,

458      Merluccius spp.(Teleostei: Gadiformes), in relation to their depth distribution and feeding. J

459      Exp Mar Biol Ecol 152, 91–104.

460  Nielsen, J.R., Kristensen, K., Lewy, P., Bastardie, F., 2014. A Statistical Model for Estimation of

461      Fish Density Including Correlation in Size, Space, Time and between Species from

462      Research Survey Data. PLoS One 9(6). doi:10.1371/journal.pone.0099151

463  Pante, E., Simon-Bouhet, B., Irisson, J.-O., 2015. marmap: Import, Plot and Analyze

464      Bathymetric and Topographic Data. R package version 0.9.2. http://CRAN.R-

465      project.org/package=marmap.

466  Payne, A.I.L., 1995. Cape hakes. Ocean. life off South. Africa. Ed. by A.I.L. Payne, R.J.M.

467      Crawford. Vlaeb. Publ. Cape Town, South Africa 136–147.

468  Payne, A.I.L., Punt, A.E., 1995. Biology and fisheries of South African hakes (M. capensis and

469      M. paradoxus). Hake Fish. Ecol. Mark. pp. 15–47. Ed. by J. Alheit, T.J. Pitcher. Chapman

470      Hall, London.

471  Rae, C.M.D., 2005. A demonstration of the hydrographic partition of the Benguela upwelling

472      ecosystem at 26° 40'S. African J. Mar. Sci. 27, 617–628.

473  Singh, L., Yolanda, M., Glazer, J., 2011. Merluccius capensis and M. paradoxus length at 50%

474      maturity based on histological analyses of gonads from surveys. DAFF Work. Gr. Doc.

475     Fish.

476     Strømme, T., Lipinski, M.R., Kainge, P., 2016. Life cycle of hake and likely management

477         implications. Rev. Fish. Biol. Fish. 26, 235–248. doi:10.1007/s11160-015-9415-9

478     von der Heyden, S., Lipinski, M.R., Matthee, C.A., 2010.  Remarkably low mtDNA control

479         region diversity in an abundant demersal fish. Mol. Phylogenet. Evol. 55, 1183–1188.

480     Wieland, K., Durholtz, M.D., Fairweather, T., 2013. Environmental effects on hake catchability

481         in the South African West Coast survey. MARAM IWS/DEC13/Ecofish/P3 1–29.

482

483

484    Table 1. Model parameter estimates and standard errors. Parameters with unit "1" are
485    dimensionless.

486

| Symbol | Description | Unit | Estimate | Standard error | CV (%) |
|---|---|---|---|---|---|
| $\ell_{50}^{Gisund}$ | Fish size at half selection (Gisund) | cm | 8.372 | 0.882 | 11 |
| $SR^{Gisund}$ | Selection range (Gisund) | cm | 1.414 | 0.308 | 22 |
| $g$ | Growth rate | cm/year | 8.320 | <0.001 | <0.001 |
| $z$ | Total mortality | 1/year | 0.325 | 0.218 | 67 |
| $\sigma_{\varepsilon}^2$ | Variance of population dynamics | 1 | 0.033 | 0.006 | 18 |
| $T$ | Decorrelation time | year | 30.088 | 2.220 | 7 |
| $L$ | Decorrelation size | cm | 79.069 | 1.894 | 2 |
| $H$ | Spatial decorrelation distance | km | 480.606 | 31.087 | 6 |
| $\sigma^2$ | Variance of the space-time-size correlations | 1 | 20.934 | 1.265 | 6 |
| $\sigma_N^2$ | Variance of the nugget effect | 1 | 12.350 | 0.283 | 2 |

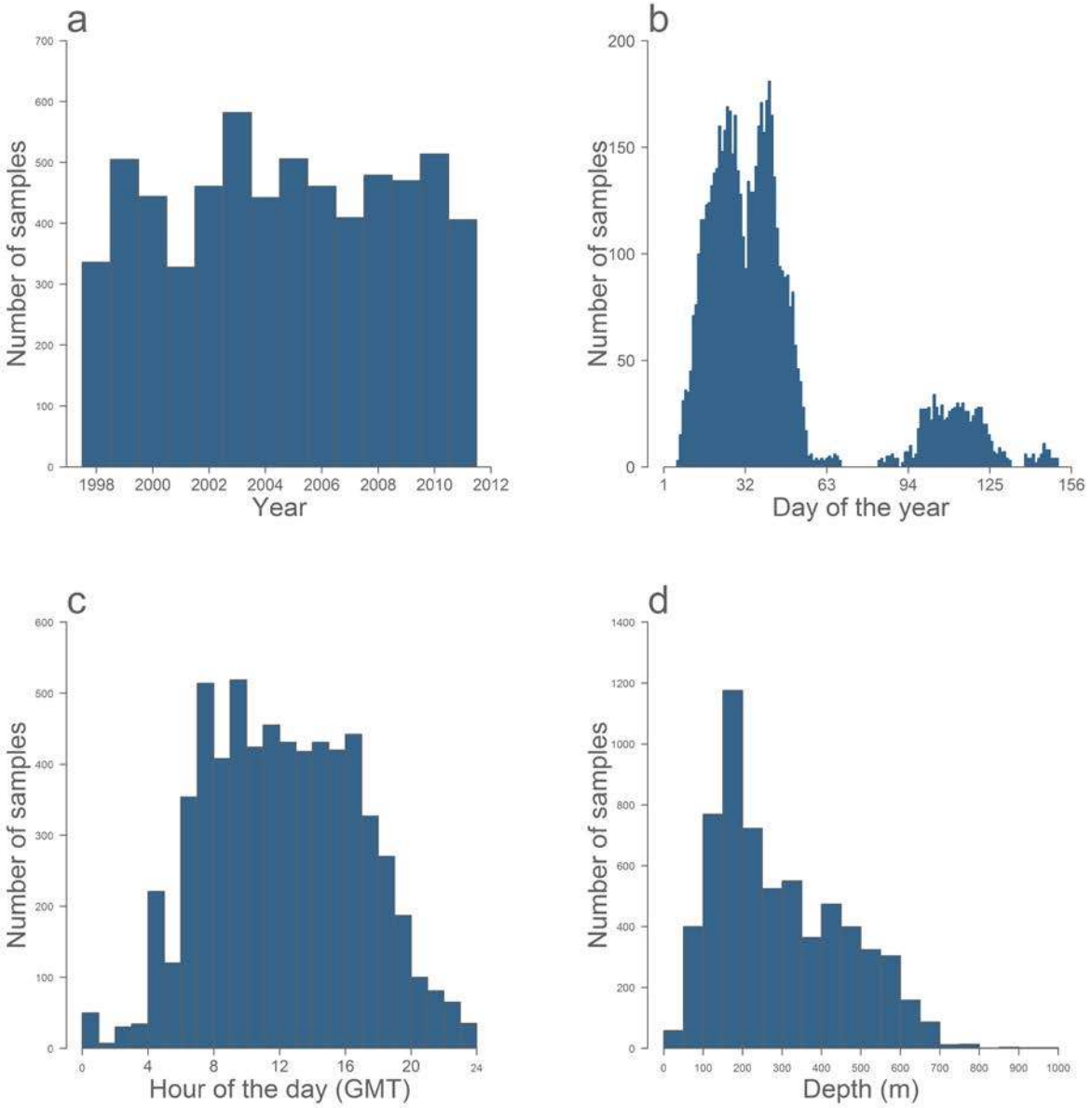487

488

489

490  **Figures**

491
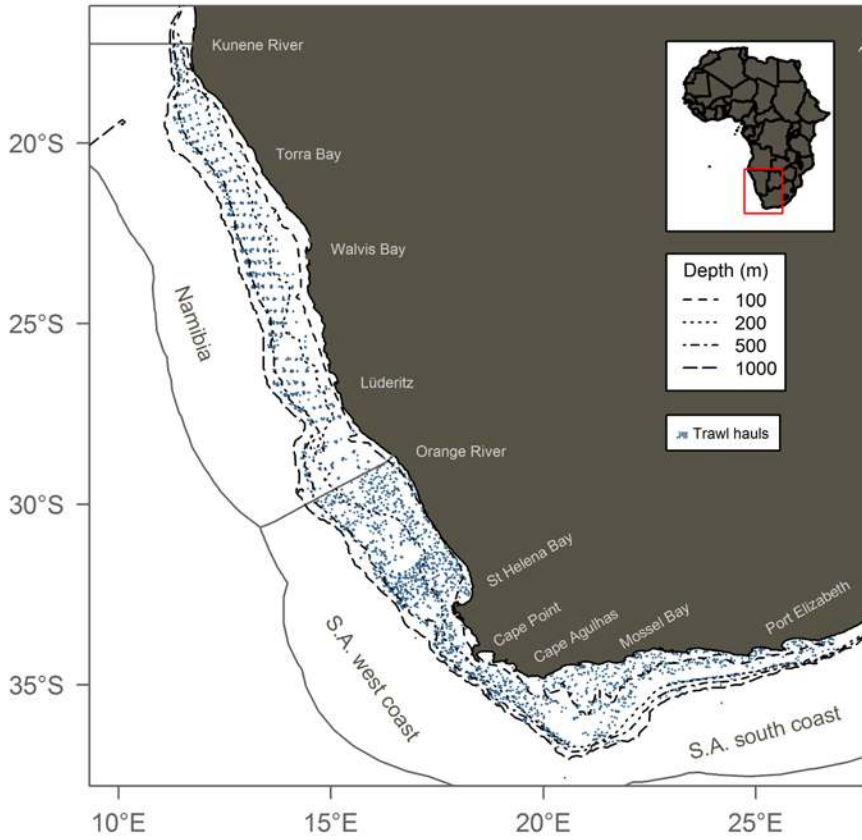


492

493  Figure 1. Map of study area with sample locations (dots), isobaths and place names referred to in
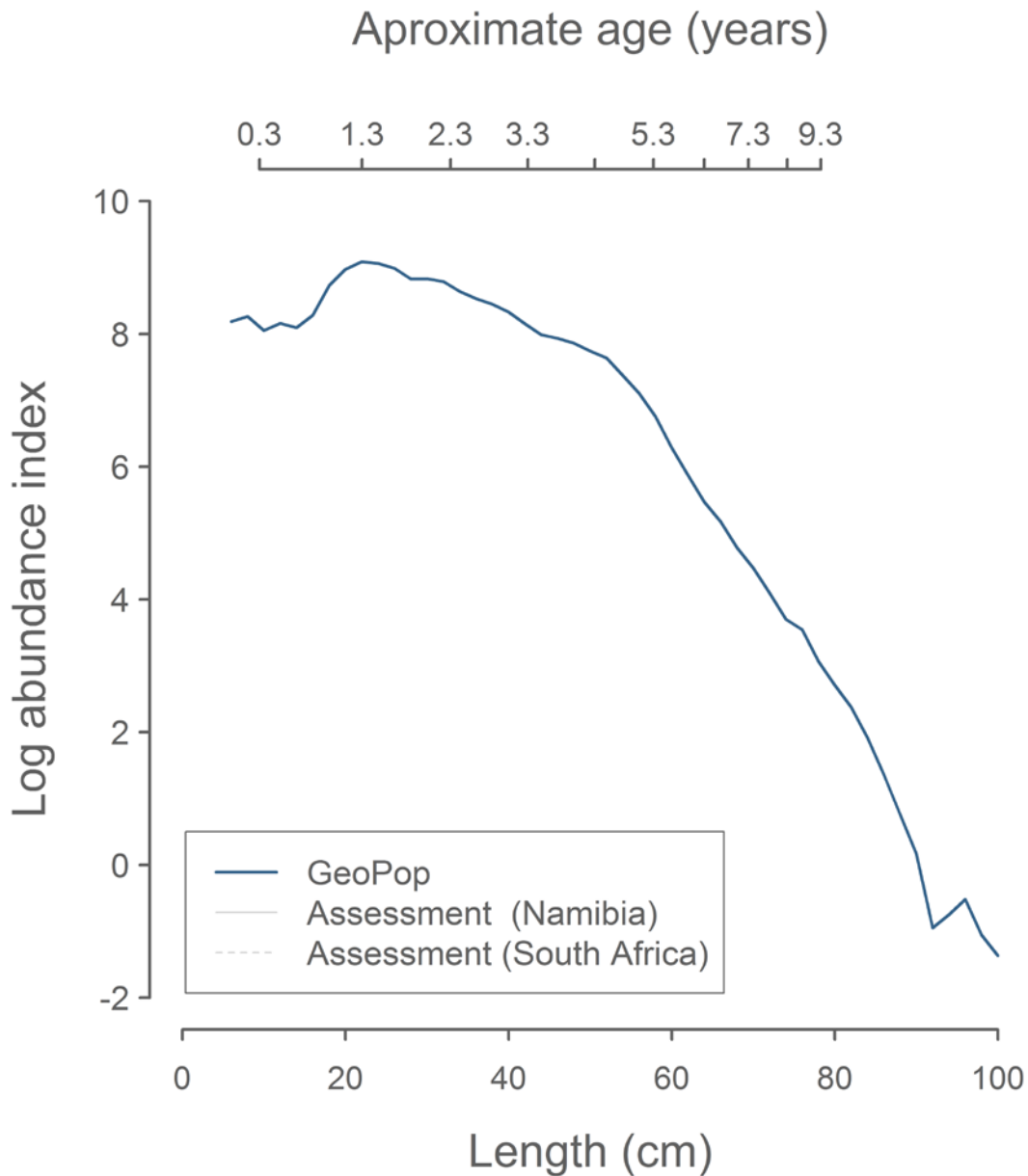
494      the text.

495

496
497 Figure 2. Demersal trawl survey samples (trawl hauls) by year (a), ordinal day (b), hour of the
498 day (c) and depth (d).
499

500
501  Figure 3. Log abundance index of deep-water hake (*M. paradoxus*) by length and approximate
502   age (blue line). Inclination equals the total mortality. The mortality estimated in the
503   Namibian and South African stock assessments are indicated by grey lines [To be added]
504   (mean Z in South Africa from 1998 to 2012 from Rademeyer (2012) and in Namibia from
505   1998 to 2011 from Kathena et al. (2015)).

506
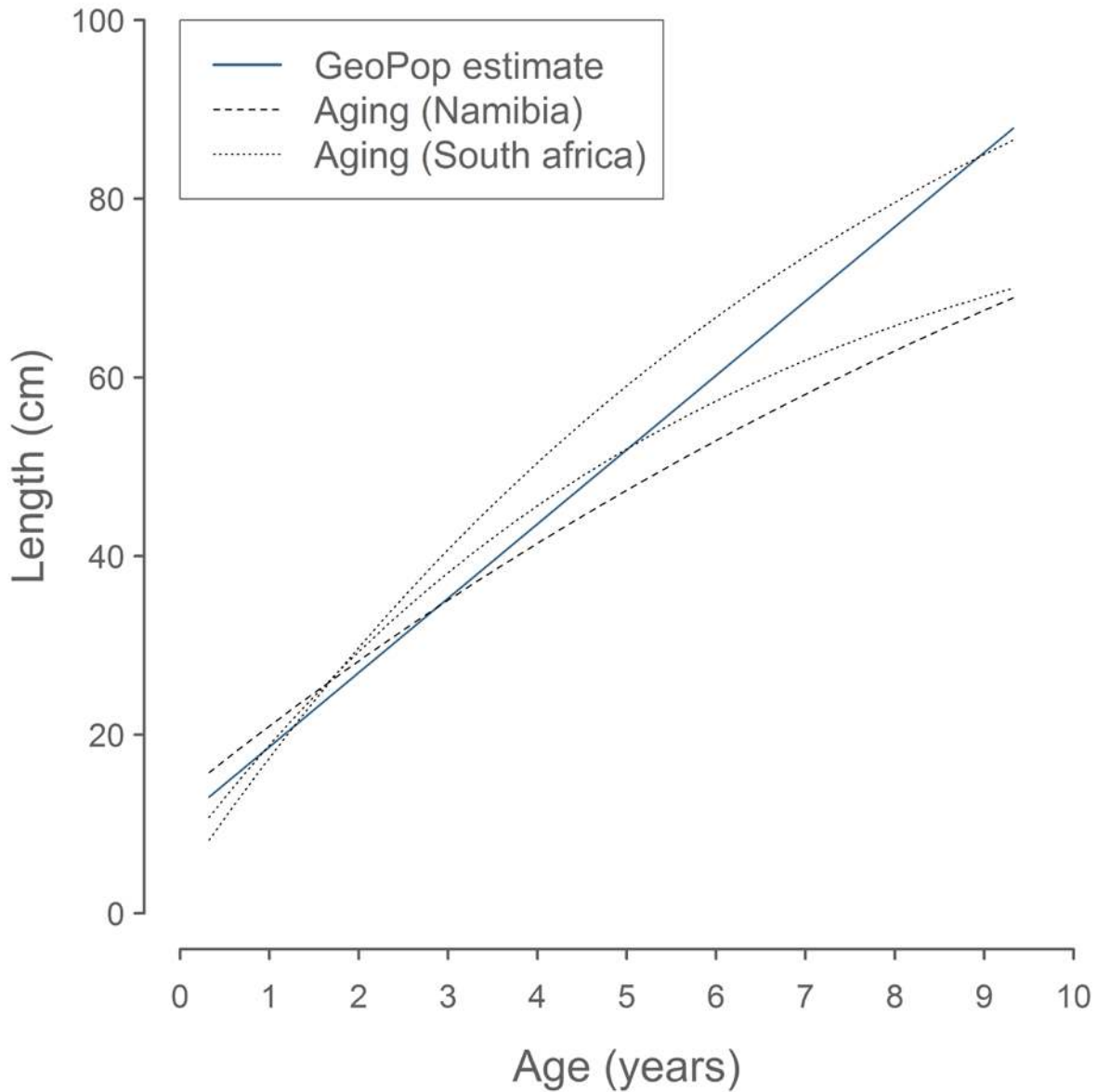
507

508    Figure 4. Comparison of growth rate estimates for deep-water hake (*M. paradoxus*). Estimate

509         from the GeoPop model (*8.4 cm year$^{-1}$from first surveyed at an age of approximately*  0.3

510         years corresponding to 9.5 cm according to South African age readings, blue straight line),

511         Von Bertalanffy equations fitted to South African age readings (females: upper dotted line;

512         males: lower dotted line), Namibian age reading (dashed line).

513
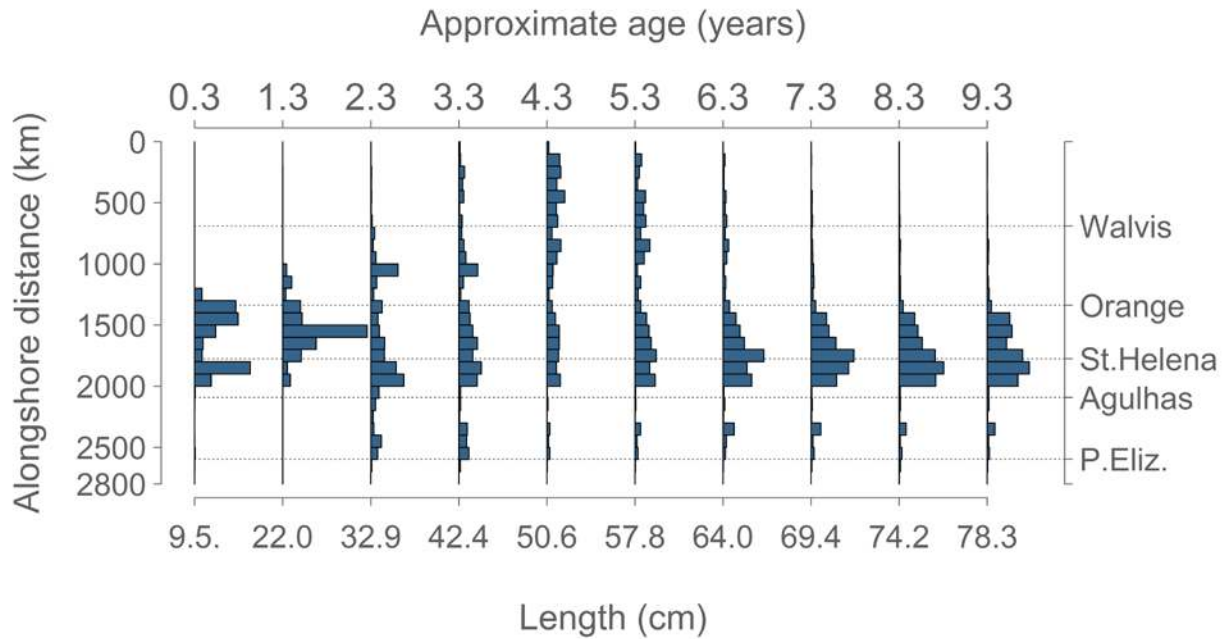
514

515    Figure 5. Alongshore distribution of number of deep-water hake (*M. paradoxus*) by length and

516        approximate age estimated by GeoPop model after removal of local noise (nugget effect).

517        The distributions are standardized for each age, so the areas of the bars are the same for all

518        age distributions. The spatial distributions were projected onto a curvilinear axis following

519        the coastline from the Namibia-Angola border (Kunene River) in the North to Port Elizabeth

520        in the south-east.

521
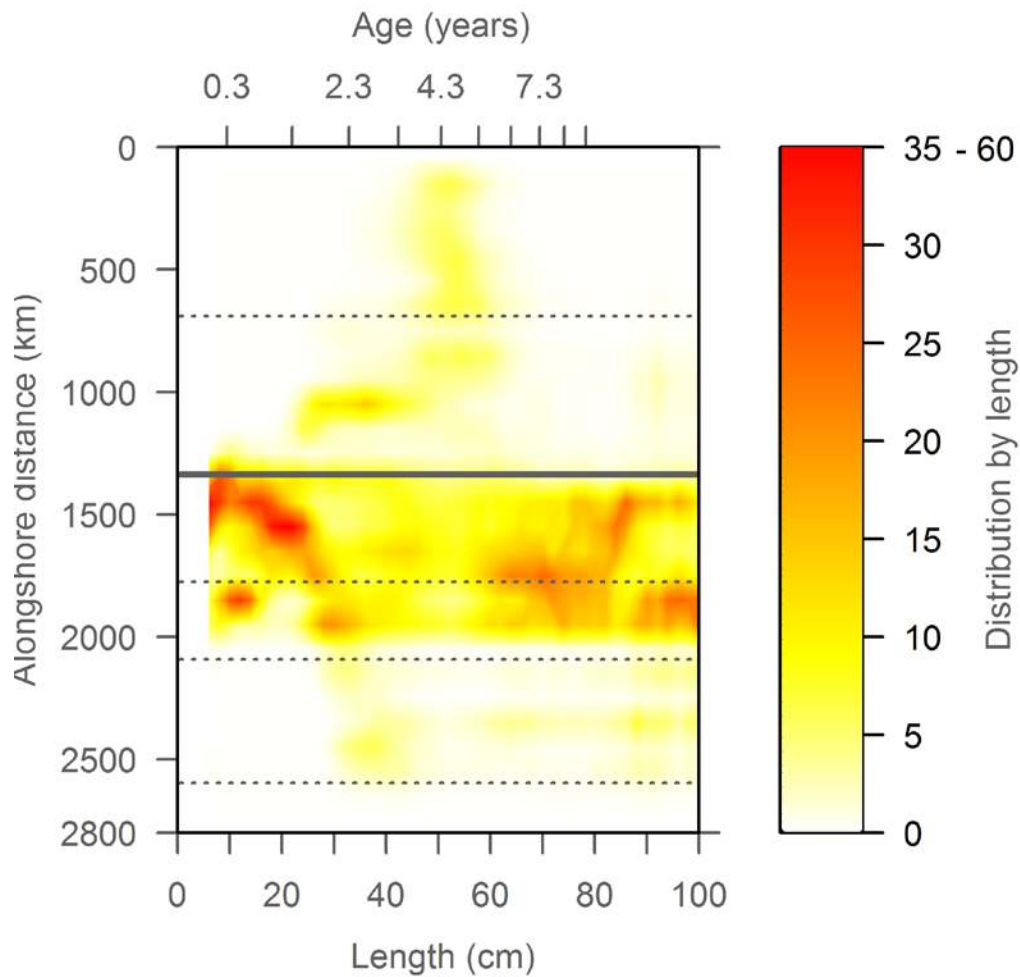
Figure 6. Alongshore distribution of number of deep-water hake (*M. paradoxus*) by length and approximate age estimated by GeoPop model after removal of local noise (nugget effect). The distributions are standardized for each 2-cm length class. The spatial distributions were projected onto a curvilinear axis following the coastline from the Namibia-Angola border (Kunene River) in the North to Port Elizabeth in the south-east.
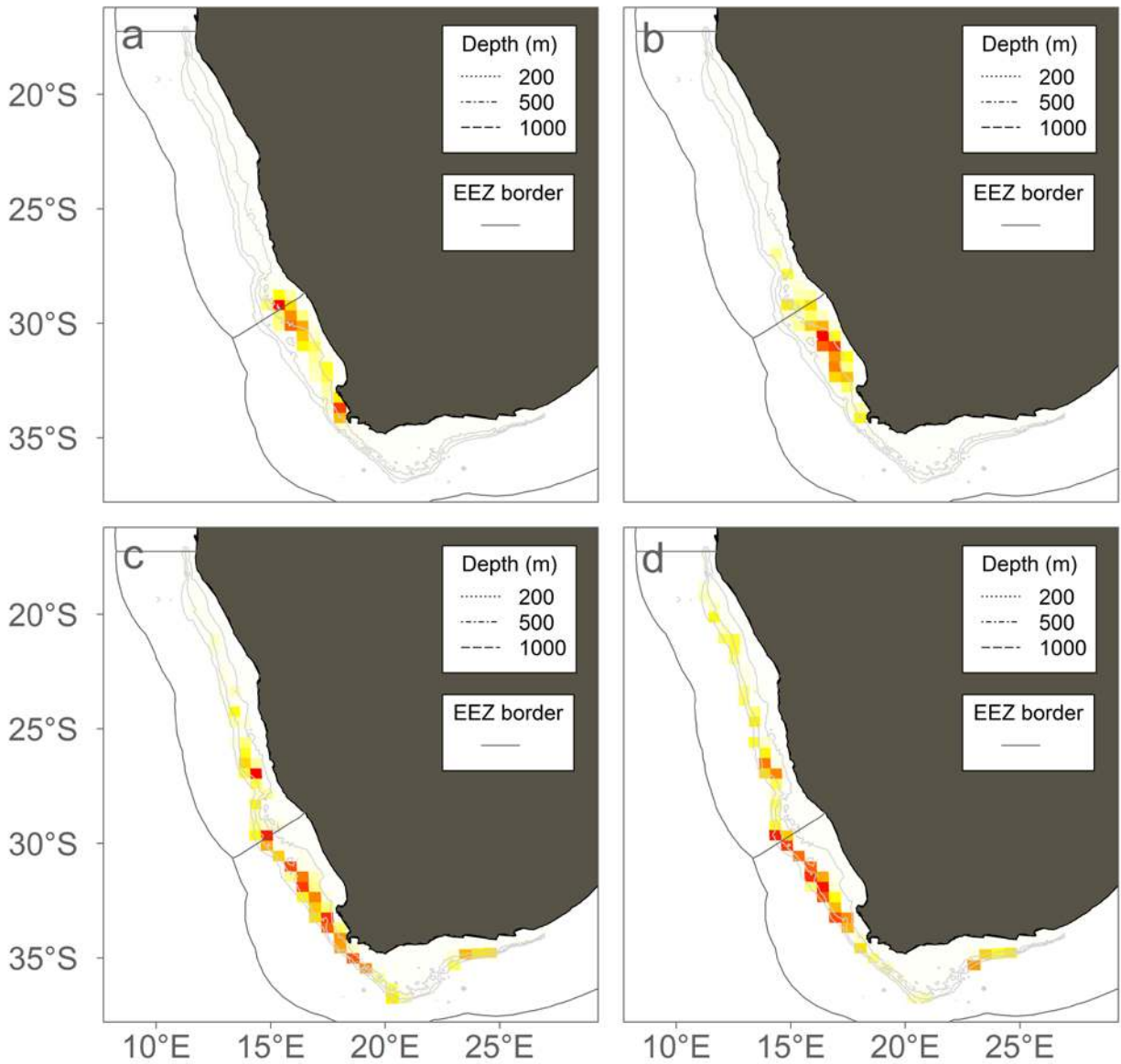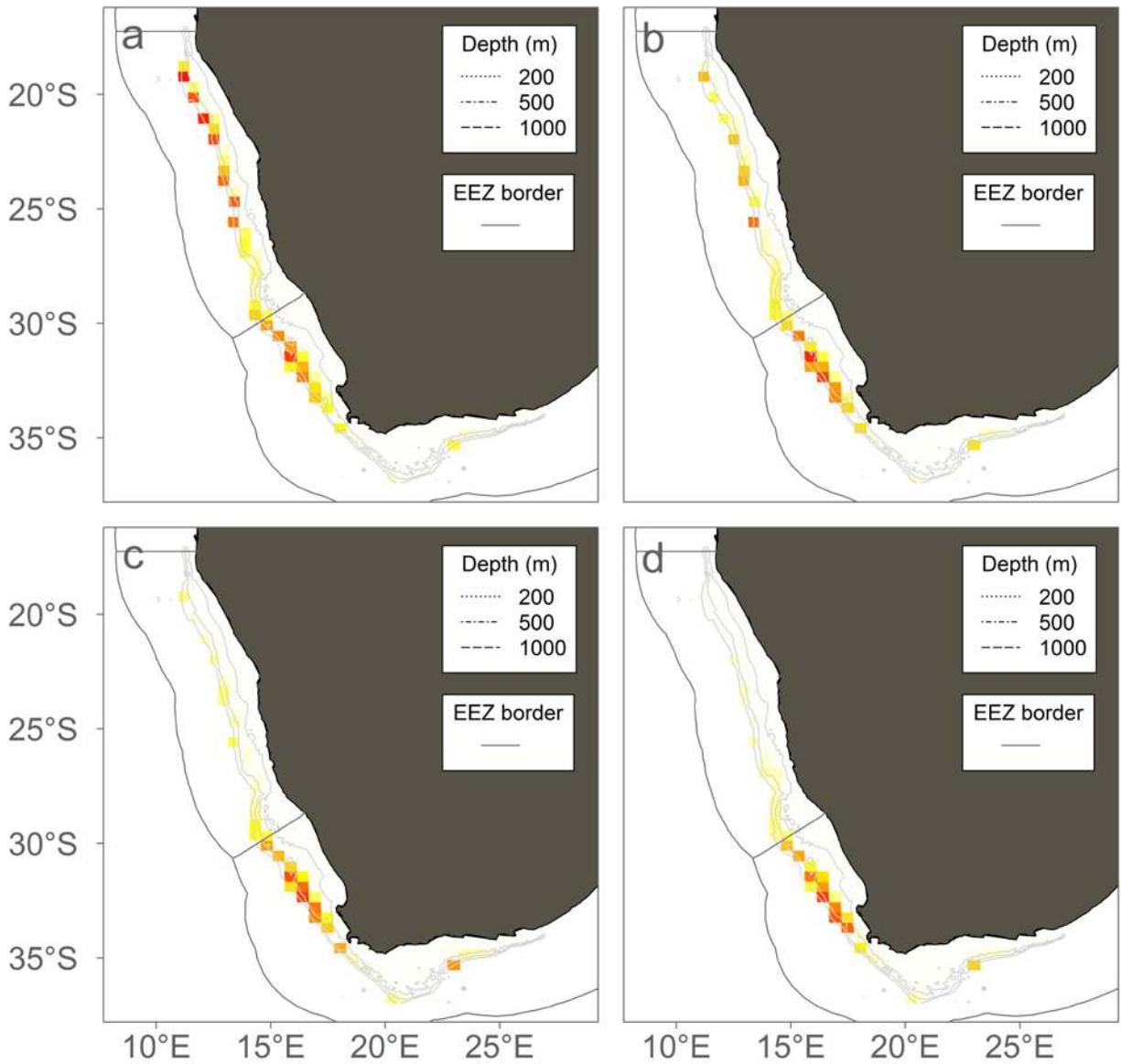
529

530 Figure 7. Distribution maps of deep-water hake (*M. paradoxus*) at the age of approximately 0.3

531 years (a), 1.3 years (b), 2.3 years(c) and 3.3 years (d). The distributions are illustrated as

532 cumulative fractions, e.g. the sum of all areas with the color corresponding to 40 %

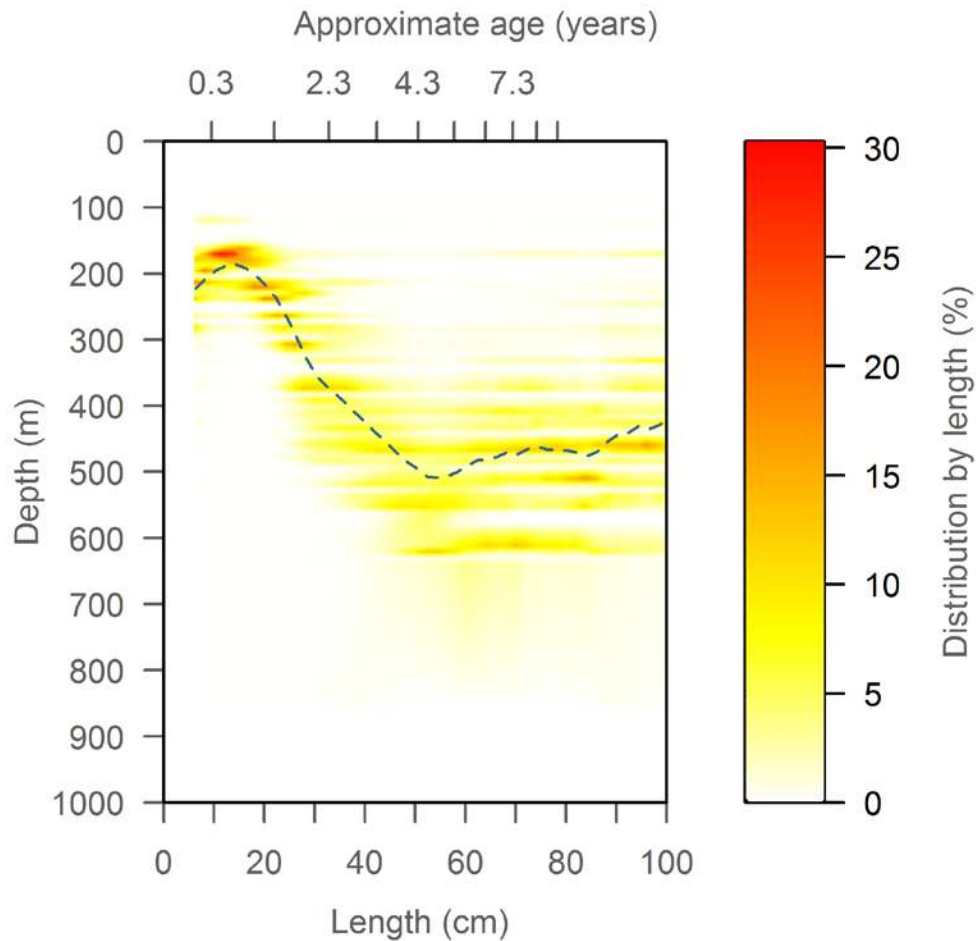533 represents 40 % of the total.

534

535

Figure 8. Distribution maps of deep-water hake (*M. paradoxus*) at the age of approximately 4.3
years (a), 5.3 years (b), 6.3 years(c) and 7.3 years (d). The distributions are illustrated as
cumulative fractions, e.g. the sum of all areas with the color corresponding to 40 %
represents 40 % of the total.

540

541

542 Figure 9. Depth distribution of deep-water hake (*M. paradoxus*) by length and approximate age.

543     Blue dashed lines indicate the weighted mean depth.

544

**Supplementary information**

546 Supplementary information 1. The gear effect on catch rates of *M. paradoxus*.

547

548 Supplementary information 2. No large scale spatial bias in nugget effect.

549

550 Supplementary information 3. Sensitivity test for the gear effect on the catch rates of *M.*

551 *paradoxus* [Not done yet].

552

553

554

**Suppl. info. 1: The gear effect on catch rates of *M. paradoxus***

As detailed in Materials and Methods, the data base for the present study includes catch rates with different gears. The study must take the difference in the size selectivity and efficiency of the different gears into account, to avoid spurious patterns and bias in the estimated spatial distributions of the stock. Here, we describe how the catches from the R/V Africana are converted to equivalent catches that we can asssume would have been obtained with Gisund. We refer to this as "gear intercalibration".

We constructed a statistical method for intercalibration, i.e. determining the relative selectivity of two gear types, based on data from paired trawl hauls. The model estimates the size spectrum of the underlying population at each station, size-structured clustering of fish at small temporal and spatial scales, in addition to the relative selectivity of the two gears in each length class. The statistical assumption is Poisson distributed catches conditional on log-Gaussian variables that describe the expected catches, which allows for overdispersion and correlation between catch counts in neighboring size classes.

**SI 1.1: Statistical model**

The intercalibration model is a statistical model which explains the size composition of the catch in survey trawl hauls. The model is a non-linear mixed effect model, in which we do inference using numerical maximum likelihood estimation, employing the Laplace approximation to integrate out random effects.

The observed quantities are count data, $N_{ijk}$, which represents number of individuals caught at station $i = 1, \ldots, n_s$, with gear $j = 1, 2$, and in length group $k = 1, \ldots, n_l$. Here, the length groups are 2 cm length classes starting at 10 cm.

We assume that these catches are Poisson distributed, conditional on the swept area $A_{ij}$ and three sets of random variables, which all depend on the size class $k$: First, the local background size spectrum $\Phi_{ik}$, which is specific to the station, second, haul-specific fluctuations $R_{ijk}$ in the size spectrum, and third, the relative selectivity $S_{jk}$ which is specific to the gear. More specifically, $\Phi_{ik}$ represents the size composition of the fish at station $i$, as would be observed with a hypothetical gear with "typical" size selectivity, so that $\exp(\Phi_{ik})$ is the expected number of fish caught in size group $k$ at station $i$ with a hypothetical gear which lies in between the two gears $j = 1$ and $j = 2$.

Next, the haul-specific fluctuations $R_{ijk}$ are akin to the "nugget effect" in spatial statistics, and represents small-scale clustering of fish. This is particular to both stations and gear, since the paired hauls are done at slightly different locations and times, and therefore these clusters have moved or regrouped between hauls at the same station.

Finally, the selectivity $S_{jk}$ is the main object of interest, and represents the selectivity of gear $j$ in size group $k$. Since we do not know the actual size

distribution of the stock, we cannot estimate the absolute selectivity, but only the relative selectivity between the two gears. This corresponds to enforcing $S_{1k} = -S_{2k}$

Given these random variables $\Phi$, $R$, $S$, we assume that count data is Poisson distributed:

$$N_{ijk}|\Phi, R, S \sim \text{Poisson}(A_{ij} \cdot \exp(\Phi_{ik} + S_{jk} + R_{ijk}))$$

The swept area $A_{ij}$ is an input to the model. The unobserved random variables, $\Phi$, $R$ and $S$, are given prior distributions: The size spectrum at each station, i.e. $\Phi_{ik}$, is considered a random walk over size groups:

$$\Delta\Phi_{ik} \sim N(0, \sigma_\Phi^2) \text{ for } k = 1, \ldots, n_l - n_\Phi \quad .$$

Here, $\Delta$ is the difference operator. This enforces continuity in the size spectrum; the most probable spectrum is flat. To ensure that the spectrum is a well defined stochastic process, we complement this with initial conditions

$$\Phi_{ik} \sim N(0, \sigma_1^2) \text{ for } k = 1 \quad .$$

Here, the variance $\sigma_1^2$ is fixed at a "large" value 10. In contrast, the parameter $\sigma_\Phi^2$ is estimated. We assume independence between stations, i.e. we do not attempt to model any large-scale spatiotemporal structure of the population. We note that this is the main difference between this model and the GeoPop model, where emphasis is exactly on this spatiotemporal structure.

The residual or "nugget effect" $R_{ijk}$ models size-structured clustering of the fish at small spacial and temporal scales. Thus, this effect is independent between hauls, even those taken at same station $i$ but with different gear $j$. For a given haul, i.e. for given station $i$ and gear $j$, the nugget effect is a mean 0 first order autoregressive process of size, with a variance $\sigma_N^2$ and correlation coefficient $\phi$ which is estimated.

The relative selectivity $S_{jk}$, which we aim to estimate, is modeled as a random walk in size:

$$\Delta S_{jk} \sim N(0, \sigma_S^2) \text{ for } k = 1, \ldots, n_l - n_S$$

We assume infinite variance on the first size group, $S_{j1}$, i.e. only the increments in the selectivity process enter into the likelihood function.

|  | Africana Old | | Africana New | |
| Parameter | Estimate | Std. Error | Estimate | Std. Error |
|---|---|---|---|---|
| $\log \sigma_\Phi$ | 0.077 | 0.02 | 0.17 | 0.02 |
| $\phi$ | 0.927 | 0.01 | 0.92 | 0.01 |
| $\log \sigma_N$ | -0.039 | 0.05 | -0.08 | 0.05 |
| $\log \sigma_S$ | -3.145 | 0.25 | -2.76 | 0.24 |

Table 1: Parameter estimates

### SI 1.2: Implementation

The statistical model in the previous defines the joint distribution of the count data, $N$, and the unobserved random variables $\Phi$, $R$, $S$, for given parameters $\sigma_S$, $\sigma_\Phi$, and the two parameters (scale and range) defining the nugget effect. The unobserved $\Phi$, $R$ and $S$ are integrated out using the Laplace approximation, to yield the likelihood function as a function of the four parameters. The likelihood function is maximized to yield estimates of the four parameters, after which the posterior means of the $\Phi$, $R$, and in particular $S$ are reported.

The computations are performed in R version 3.1.2 (R Core Team, 2015); we use the Template Model Builder (TMB) package (Kristensen et al., 2016) for evaluating the likelihood function and its derivatives.

### SI 1.3: Data

The data base consisted of a total of 236 pairs of trawl hauls performed by RVs Africana and Dr. Fridtjof Nansen. The Gisund gear was used onboard Fridtjof Nansen, while RVs Africana deployed two gear types: "Africana Old" (108 hauls) and "Africana New" (128 hauls). Catch in numbers per length group and the swept area (hauling distance multiplied by wing spread) were available for each haul.

### SI 1.4: Results

The obtained intercalibration curves are seen in figure 1. Notice that Gisund overall is more effective than both the Old and the New Africana, in particular in the small size classes. The difference between size classes is statistically significant ($p < 10^{-4}$). For size classes larger than 30 cm, say, the intercalibration curves show little variation with size and although this has not been tested, it is plausible that these variations are not statistically significant. Estimated parameters are seen in table 1.

# References

Kristensen K, Nielsen A, Berg C, Skaug H (2016) TMB: Automatic differentiation and Laplace approximation. *J. Stat. Softw* 70.
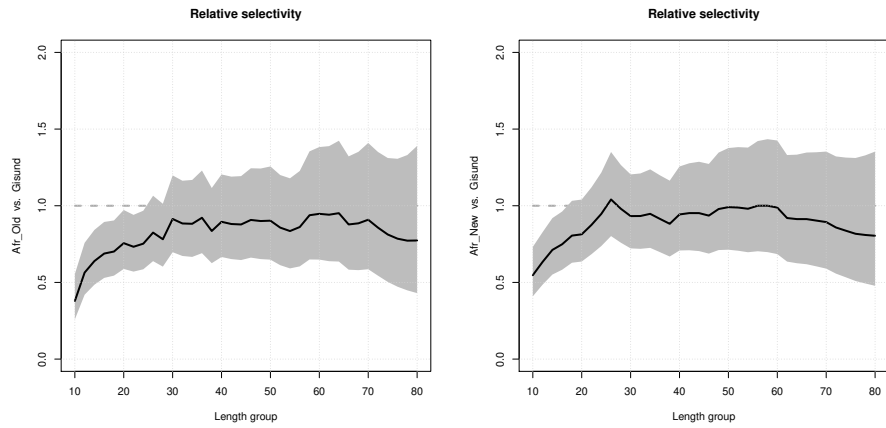
Figure 1: Relative selectivity (gear calibration factor), comparing catches of M. paradoxus with Gisund gear and the "Old" and "New" gear on the R/V Africana. Large values indicate that Africana is more effective. Solid curve: Estimated relative selectivity (posterior mode). Grey region: Marginal 95 % confidence intervals.

R Core Team (2015) *R: A Language and Environment for Statistical Computing* R Foundation for Statistical Computing, Vienna, Austria.
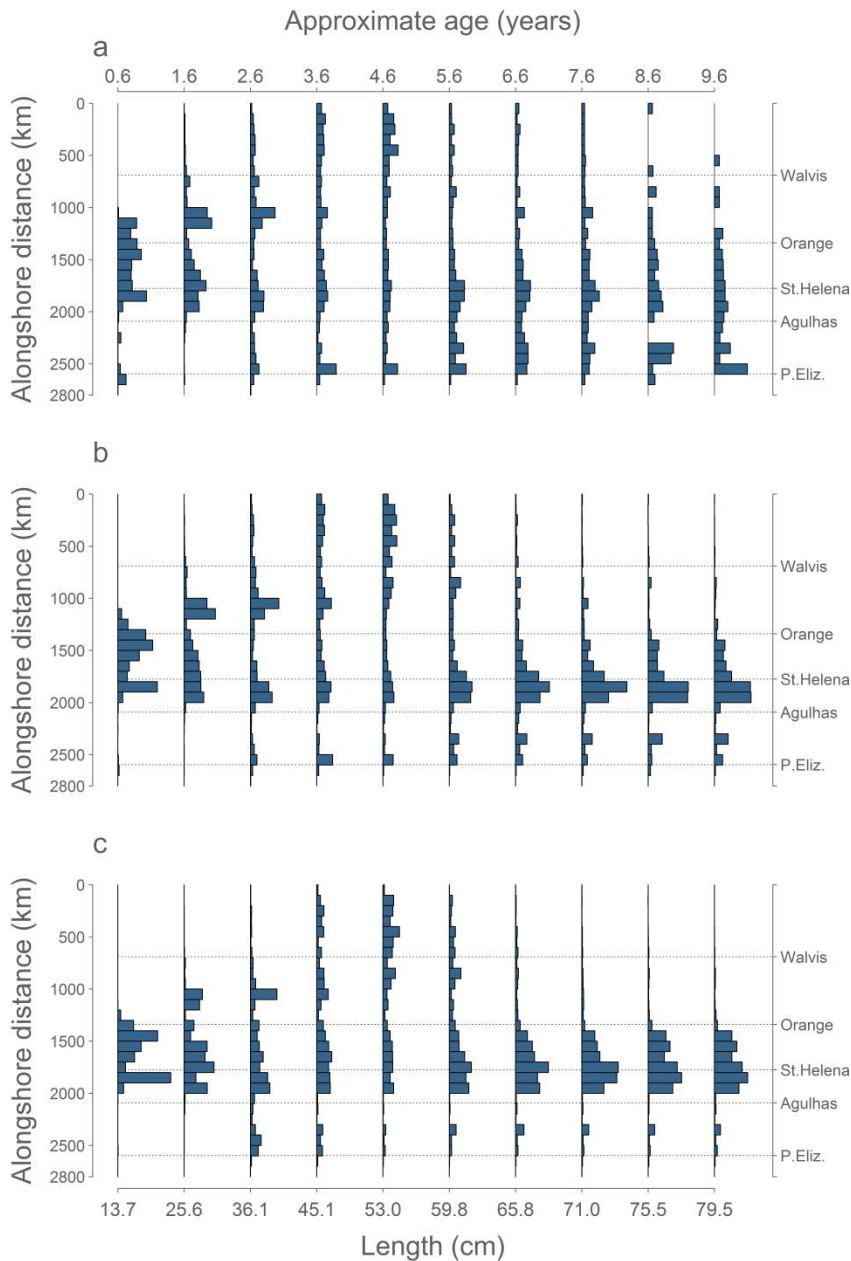
# Supplementary information 2



Figure SI2.1. Alongshore distribution of number of deep-water hake (*M. paradoxus*) by size and approximate age. Simple average of catches (a), GeoPop model fit (b) and GeoPop model after removal of local noise (nugget effect) (c). The spatial distributions have been projected onto a curvilinear axis following the coastline from the Namibia-Angola border (Kunene River) in the North to Port Elizabeth in the south-east. This figure is made for comparison with figure 5 in Jansen et al. (2016) and is therefore made in the same design (Jansen et al., 2016).